Molecular Catalysis 547 (2023) 113333

Contents lists available at ScienceDirect

Molecular Catalysis

journal homepage: www.journals.elsevier.com/molecular-catalysis

Surface modification of Fe_5C_2 by binding silica-based ligand: A theoretical explanation of enhanced C_2 oxygenate selectivity

Junqing Yin [a,c,*], Shuyuan Wang [b], Dan Xu [b], Yong You [a], Xingchen Liu [d], Qing Peng [e]

[a] Institute of Advanced Study, Chengdu University, Chengdu 610106, China
[b] Energy Research Institute, School of Energy and Power Engineering, Qilu University of Technology, Jinan 250014, China
[c] National Energy Canter for Coal to Liquids, Synfuels China Co., Ltd., Huairou District, Beijing 101400, China
[d] State Key Laboratory of Coal Conversion, Institute of Coal Chemistry, Chinese Academy of Sciences, Taiyuan 030001, China
[e] State Key Laboratory of Nonlinear Mechanics, Institute of Mechanics, Chinese Academy of Sciences, Beijing 100190, China

ARTICLE INFO

Keywords:
Surface modification
Iron carbide
Support-like ligand
Catalytic selectivity
Fischer-Tropsch Synthesis

ABSTRACT

Elucidating the role(s) of support-like ligands remains a challenge in catalytic reaction like the Fischer-Tropsch Synthesis (FTS) catalyzed by the iron catalyst supported on silica. We herein theoretically investigated surface modification of Fe_5C_2 by silica-based ligand and its influence on C_2 oxygenate selectivity in FTS, by carrying out DFT calculations on dissociation of CO and formations of CH_4 and C_2 on *ha*-SiO_2/Fe_5C_2(510). To mimic the structure of surface modification, the *ha*-SiO_2/Fe_5C_2(510) model was built up by binding the silica cluster (the *ha*-SiO_2 ligand) to Fe_5C_2(510). DFT calculations elucidated that the C + CH coupling with the lowest activation barrier among all the possible routes of C_2 formation on Fe_5C_2(510) is suppressed after modification with the *ha*-SiO_2 ligand because the binding *ha*-SiO_2 ligand limits the geometry relaxation caused by the C+CH coupling. However, CO molecule is anchored by the *ha*-SiO_2 ligand via hydrogen bond, suppressing the C—O cleavage because the *d*-valence band center of Fe_5C_2(510) lowers in energy by surface modification with the *ha*-SiO_2 ligand, but facilitating the C + CO coupling with the lowest activation barrier among all the possible routes of C_2 formation. Also, CH_4 formation in the *ha*-SiO_2/Fe_5C_2(510) case is not so easy as that on Fe_5C_2(510). Therefore, C_2 oxygenate is formed more easily in the *ha*-SiO_2/Fe_5C_2(510) case than in the Fe_5C_2(510) case. The result agrees with the experimental observation that C_2 oxygenate selectivity became high for iron-based FTS catalyst after surface modification of by silica-based ligand.

1. Introduction

Interface metal-support interaction (IMSI) is developed as a collective term describing effects introduced by the intimate contact between the metal and support, claimed from both the reducible and non-reducible supports [1–3]. The reducible supports often cause drastic changes in the shape and electronic properties, chemisorption properties, and catalytic performance of metal nanoparticles [4–6] while the influence of non-reducible supports on the catalytic performance is usually regarded to be not so obvious as that of reducible supports. However, silica, as a typical non-reducible support, plays an important role in improving resistance against sintering of iron-based catalysts in the industry of iron-based Fischer-Tropsch Synthesis (FTS) [7,8]. To improve the performance of traditional iron/silica catalyst, investigations have been made on the usage ratio of syngas [9], the activation conditions [10,11], the shape and size of particles [12,13], the composition of iron phases [14–16], and the promoter [17,18] and support effects [19,20] of catalyst itself. In these researches, it was found that silica influences the catalytic activity and catalytic selectivity in the FTS process [21–23]. For instance, CH_4 selectivity was improved when the Fe-based FTS catalyst incorporates with silica [24,25], whereas CH_4 selectivity decreases with a proper amount of silica in co-precipitated iron/silica catalysts [26]. The existed controversies are related to the variation of the iron-silica interface structure and other factors such as the changes in the size, morphology, and phase of iron species but it is hard to obtain the clear structure and evaluate the exact activity of iron-silica interface in practice [27–29]. It is indispensable to understand the electronic structure and catalytic activity of the iron-silica interface for tuning the performance of silica-supported iron-based (named iron/silica) FTS catalysts, but the knowledge is insufficient.

* Corresponding author at: Institute of Advanced Study, Chengdu University, Chengdu 610106, China.
E-mail address: yinjunqing@cdu.edu.cn (J. Yin).

https://doi.org/10.1016/j.mcat.2023.113333
Received 15 March 2023; Received in revised form 5 June 2023; Accepted 20 June 2023
Available online 29 June 2023

Recently, surface modification by binding ligands on catalyst has attracted growing interest as one of effective approaches to enhance the stability of metal catalysts and to investigate the IMSI influence on the performance of metal catalysts in reactions such as cyclohexene oxidation [30], CO oxidation [31,32], and CO_2 reduction [33], dimethyl oxalate hydrogenation to ethylene glycol [34], methanol synthesis from CO_2 [35], and also in FTS [36–38]. For instance, Chaudret et al. [36] found that the diphosphine ligands stay on the surface of Ru nanoparticles during FTS reaction and improve their selectivity toward C_2–C_4 hydrocarbons. In the theoretical work by Heerden et al. [37], an inversed model was constructed by binding the cluster model of the support on the metal catalyst surface to mimic the surface modification of metal catalyst by support-like ligands. They concluded that the surface modification of Co by binding alumina-based ligands increases the exposure ratio of Co(100) and Co(111), altering the crystallite morphology. DFT calculations by Zhang et al. [39] also demonstrated that carbon chain growth depends on the crystallite morphology and bulk phase. Therefore, the surface modification strategy is helpful to acquire the knowledge of the metal-support interface performance in heterogeneous catalysis.

In the silica-supported iron-based FTS, silica could be transported over the surface of iron nanoparticles under a certain pressure of steam [40,41], providing us a concept that a silica-like ligand may inevitably bind to the surface of silica-supported iron nanoparticles. On the base of this concept, Mogorosi and Steen et al. [42] employed an inverse catalyst model to experimentally study the reactivities on the iron-silica interaction in FTS by modification of nano-sized iron catalysts with well-dispersed silicate groups confirmed by infrared spectra. They found that the CO adsorption strength was reduced but the availability of hydrogen on the catalyst surface was enhanced. A similar iron-based catalyst prepared by Kishida et al. [43] produced C_2 oxygenates with an extremely high selectivity, compared to the impregnation catalyst. Even so, hydrocarbons remain the main product for the iron-based FTS catalyst in the most cases. There is an open question: why formation of C_2 oxygenates become easy after modifying the catalyst with silica-like ligand? One of possibilities we proposed is that the large change in the selectivity of C_2 oxygenates likely happens when the catalyst surface of χ-Fe_5C_2 was modified by silica-based ligands, because of two reasons as below. One, χ-Fe_5C_2 is the well-known active phase for carbon chain growth in the iron-based FTS. The other, the silica-based ligands influence the performance of silica-supported iron-based FTS catalyst much more than the case of silica acting as the general inert support. From the viewpoint of the surface science, it is important to predict how the catalytic performance is changed and elucidate the reason why the catalytic performance is improved by binding support-like ligand on the surface of catalysts. In this case, some open questions exist: (*i*) what is the stable structure of the silica-ligand on the Fe_5C_2 surface and how about the electronic properties of the Fe_5C_2 surface with the silica ligand? (*ii*) how does the reactivity of CO dissociation influence and the reason why? (*iii*) why does the selectivity of the C_2 oxygenates become high in the presence of the silica-ligand?

To answer the above questions, the surface modification strategy was used to theoretically study the FTS reactions at the interface of silica and χ-Fe_5C_2 in this work. We employed the Fe_5C_2(510) surface because the Miller index surface (510) taking up a large percentage among the exposed crystal facets of χ-Fe_5C_2 was experimentally detected by XPS and HRTEM [19,44,45], and theoretically adopted to study CH_4 formation [46,47]. It is feasible and important to compare the catalytic performance of Fe_5C_2(510) before and after surface modification by binding silica-based ligands. Therefore, the strategy was achieved by adopting the inversed model *ha*-SiO_2/Fe_5C_2(510), which was constructed by binding the hydrated silica-based ligand *ha*-SiO_2 on Fe_5C_2(510). On the *ha*-SiO_2/Fe_5C_2(510) interface, the reactivity of CO dissociation was investigated. To understand the formation mechanism of C_2 oxygenates, C_2 formation was calculated by following the carbide and CO-inserted mechanisms. To evaluate the selectivity of C_2 oxygenates, the activation barrier of C_2 oxygenates was compared to those of CH_4 and other C_2 formations. The results in the *ha*-Si-O_2/Fe_5C_2(510) case were compared with those in the Fe_5C_2(510) case to show the influence of surface modification by binding silica-like ligand on the C_2 oxygenate selectivity.

2. Methods and models

2.1. Methods

DFT calculations were conducted by using Vienna ab initio simulation package (VASP) [48,49]. The interaction between electron and ion was obtained with the projector augmented wave method [50,51]. The electron exchange-correlation energy was computed under the generalized gradient approximation in the Perdew-Burke-Ernzerhof functional [52]. The kinetic energy cut of 400 eV, a first-order Methfessel-Paxton [53] electron smearing with $\sigma = 0.2$ eV and a Monkhorst–Pack *k*-point grid [54] of $2 \times 2 \times 1$ were kept in all calculations. The geometry optimization was converged with the thresholds of 0.02 eV/Å and 10^{-4} eV for forces and energy difference, respectively. Transition states were found by the nudged elastic band method [55] and confirmed by vibrational frequencies analysis at the same theory level. The density of states (DOS) was calculated using the Gaussian smearing scheme with the smearing width of 0.01 eV. [56]. Bader charge was calculated by using the program compiled by the Henkelman group [57]. The configuration stability of the silica-modified surface was checked through *ab into* molecular dynamic simulation by sampling the canonical ensemble employing Nosé–Hoover thermostats [58] with a time step of 1 fs during 4 ps of a well-equilibrated trajectory.

2.2. Models

The χ-Fe_5C_2 bulk structure in C2/c symmetry was rationalized with a *k*-points grid of $2 \times 6 \times 5$ [59]. The crystallographic parameters a, b, c, and β were determined as 11.545 Å, 4.496 Å, 4.982 Å, and 97.6°, respectively, and magnetic moment was 1.73 μ_B, agreeing reasonably with the available data in experiment [60]. The used size $p(3 \times 1)$ of Fe_5C_2(510) supercell with the vacuum region of 15 Å contains 90Fe/36C atoms, of which the upmost 60Fe/24C atoms were relaxed and the other atoms were kept in the bulk position [54]. Table S1 validates applicability of the used slab model because the checked thickness influence little on the energy change in C + CH → CCH and C + CH_2 → CCH_2 reactions.

Ring sizes of *a*-SiO_2, represented by the number *n* of Si atoms in the rings, distributes from 2 to 6. It was reported that the 2-membered silica ring is much less stable than the higher-membered ones [61]. Herein, the ring sizes from 3 to 6 were considered for the silica ligand on the Fe_5C_2(510) surface, which also ensured the surface loading of Si atoms dropping into the range (less than 4.5 atoms per nm^2) evaluated by Mogorosi and Steen et al. [42] in their "inversed" experiment. Because the residual –OH groups are still presented after the high temperature calcination [62], it is reasonable to saturate the SiO_4 tetrahedron by H atoms, affording $Si(OH)_4$. Then, the interface model of *ha*-Si-O_2/Fe_5C_2(510) was produced by the dehydration-dehydrogenation reaction [63] with the formation of Fe–O–Si bonds between the gaseous Si $(OH)_4$ molecules and the Fe_5C_2(510) surface (M):

$$M\ (s) + n\ SiO_4H_4\ (g) \rightarrow MSi_nO_{3n}H_n\ (s) + nH_2O\ (g) + 0.5n\ H_2\ (g)$$

The formed $MSi_nO_{3n}H_n$ structure corresponded to the interface model of *ha*-SiO_2/Fe_5C_2(510) employed in this work and its thermodynamic stability was assessed by the enthalpy change (E_{ave_n}) of the dehydration-dehydrogenation reaction averaged by the number *n* of Si atoms. The E_{ave_n} term was calculated by the following equation:

$$E_{ave\_n} = [E(MSi_nO_{3n}H_n)]/n + E(H_2O) + 0.5\ E(H_2) - [E(M)]/n - E(SiO_4H_4)$$

where E(x) is the total energy of X for the slab M, free H_2O, H_2, and SiO_4H_4 molecules, and the interface structure $MSi_nO_{3n}H_n$. The more negative value of E_{ave_n} means the more stable $MSi_nO_{3n}H_n$.

Energetic profiles of CH_4 formation by surface C hydrogenations take two gaseous H_2 molecular as a reference. For the elementary reaction of $CH_i + H \rightarrow CH_{i+1}$ with the reaction energy $E_{r,i+1}$ and activation barrier $E_{a.i+1}$, the relative energy (*RE*) of $CH_i + H$ is $4E_{ads(H)} + \sum E_{r,i}$. Energetic profiles of $C_1 + C_1$ coupling are started with the adsorption energy of six H atoms with three gaseous H_2 molecules as a reference. For the C—C bond formation reaction by $CH_x + CH_y$ coupling, the *RE* of $CH_x + CH_y$ is $6E_{ads(H)} + E_{r,x} + E_{r,y}$ where the $E_{r,x}$ is for $C + xH \rightarrow CH_x$ in the presence of CH_y and vice versa for $E_{r,y}$, the $E_{r(x,y)}$ and $E_{a(x,y)}$ are the reaction energy and activation barrier, respectively. The *RE* of the IS for $CO + CH_z$ coupling is $6E_{ads(H)} + E_{r,z}$, where $E_{r,z}$ is the reaction energy for $C + zH \rightarrow CH_z$ in the presence of CO.

3. Results and discussions

3.1. The Fe_5C_2(510) and ha-SiO_2/Fe_5C_2(510) structures

The interaction between *ha*-SiO_2 and Fe_5C_2(510) occurs through Fe-O-Si bonds, with SiO_4 tetrahedrons binding with each other via Si–O–Si bonds at the corners. As shown in Fig. 1(a), on the clean Fe_5C_2 (510) surface, there are Top (**T**), Bridge (**B**), 3-fold (**3F**) and 4-fold (**4F**) sites formed by Fe atoms for bonding with the O atoms of *ha*-SiO_2. The O atoms directly participating interfacial interaction are regarded as the interfacial O atoms. The possible configurations and the averaged reaction energies E_{ave_n} of *ha*-SiO_2/Fe_5C_2(510) are given in Fig. S1 of the SI. The result shows that the E_{ave_n} value is the most negative in the $n = 4$ case, indicating that the 4-membered Si ring is more stable than the other sized Si rings on the Fe_5C_2(510) surface. In the 4-membered *ha*-SiO_2/Fe_5C_2(510), the Si loading is 2.12 Si atoms per nm^2, which falls into the experiment range (0 ~ 4.5 Si atoms per nm^2) reported by Mogorosi et al. [42]. The stability of the 4-membered *ha*-Si-O_2/Fe_5C_2(510) configuration under the reaction temperature (523 K) has been verified by using *ab into* molecular dynamic simulation in this work, as shown in Fig. S2 of the SI. Thus, it makes sense for the 4-membered *ha*-SiO_2/Fe_5C_2(510) as a candidate model of the interface between the Fe_5C_2(510) and silica. Next, all the discussions about the *ha*-SiO_2/Fe_5C_2(510) case are based on the 4-membered *ha*-Si-O_2/Fe_5C_2(510) model.

In the most stable 4-membered *ha*-SiO_2/Fe_5C_2(510), as shown in Fig. 1(b), three interfacial O atoms bind at the 3F sites and one interfacial O atom binds at the B site. The average length of the Si–O bonds in the Si–O–Si is 1.64 Å (Table S2 of the SI), which agrees with the experiment value (around 1.62 Å) reported by Mozzi et al. [64]. The average bond angle of interface O–Si–O bonds (110.8°) is larger than 109.5°, indicating that stretching strain exists in the silica ring. Stretching frequencies within 758 ~ 838 cm^{-1} and 842 ~ 901 cm^{-1} are contributed by both the Fe–O–Si and Si–OH, while those within 929 ~ 964 cm^{-1} and 3792 ~ 3821 cm^{-1} are caused respectively by Si–OH and SiO—H. The frequencies 597 ~ 716 cm^{-1} for Si–O–Si symmetric stretching and frequencies 988 ~ 1078 cm^{-1} for O–Si–O asymmetric stretching suggest amorphous properties of *ha*-SiO_2 on Fe_5C_2(510). The latter is close to the reported typical adsorption band at 1020 cm^{-1} by the oligomeric silicate species and at 1090 cm^{-1} by the asymmetric O–Si–O vibration [65,66].

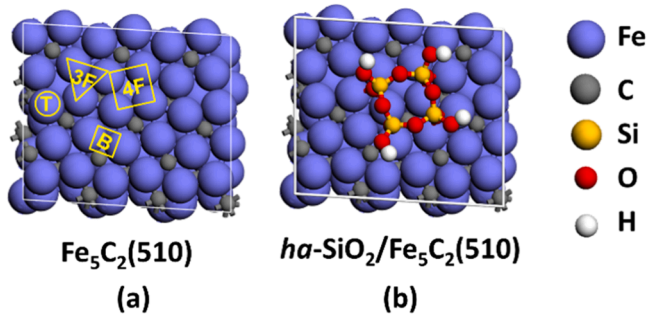

Fig. 1. The structures of the Fe_5C_2(510) surface (a) and 4-membered *ha*-SiO_2/Fe_5C_2(510) interface (b).

The Bader charge shows that in the upmost surface of Fe_5C_2(510), Fe atoms are positively charged by 0.40 *e* which is less positive than that of 0.48 *e* for the Fe atoms slightly below the upmost Fe atoms. After binding the 4-membered *ha*-SiO_2 ligand, charge transfer occurs by 2.40 *e* from the surface Fe to the ligand SiO_2, causing the bonded Fe atoms with an averaged more positive charge 0.64 *e*. In spite of these charge transfers, the Fermi level (ε_F) moves to a higher energy from –4.91 eV in the Fe_5C_2(510) case to –4.83 eV in the *ha*-SiO_2/Fe_5C_2(510) case, because the surface structures are greatly different. DOS analysis shows that spin-polarization of the top-layer atoms in Fe_5C_2(510) is considerably reduced after binding the *ha*-SiO_2 ligand, as shown in Fig. 2(a) and (b). Compared to the Fe_5C_2(510) case, the β electrons above the Fermi level are reduced obviously, suggesting that the spin-pairing interaction between the Fe_5C_2(510) and the *ha*-SiO_2 ligand occurs with unpaired electrons of the Fe and O atoms. When going from the Fe_5C_2(510) case to the *ha*-SiO_2/Fe_5C_2(510) case, the *d* band center ($\varepsilon_{dc\text{-}tot}$) decreases in energy from –6.45 eV to –6.81 eV and the *d* valence-band center ($\varepsilon_{dc\text{-}VB}$) decreases from –7.26 eV to –7.28 eV, respectively, indicating that the charge transfers from the surface to adsorbates become weak.

3.2. CO dissociation

CO dissociation starts up the FTS process. On Fe_5C_2(510), the **T**-site CO with the binding energy E_b of –2.13 eV is more stable than those at the **4F**- and **3F**-site (–2.02 eV and –1.95 eV, respectively) as shown in Fig. S3 (a) of the SI. Compared to the gaseous CO, adsorption of CO at the **4F** site causes the C–O bond extended most by 0.08 Å, which is regarded as the initial state of CO dissociation. CO dissociation can follow direct and H-assisted routes. The latter proceeds via the HCO intermediate by C-end hydrogenation and the COH intermediate by O-end hydrogenation. The mechanism via the HCO intermediate occurs more easily with the lower activation barrier E_a than that by the COH intermediate [67,68]. As shown in Figs. 3 and S4 (a) of the SI, the **4F**-site CO dissociation needs the E_a 1.17 eV by the direct route. In the H-assisted route via forming the HCO intermediate, HCO formation needs the E_a 1.45 eV with an endothermicity by 0.89 eV; cleavage of the C—O bond in HCO needs a low E_a 0.57 eV but is strongly exothermic (1.33 eV). Thus, the E_a value (1.46 eV) for CO dissociation via the HCO intermediate is larger than that by the direct route, similar to the reported result by Pham et al. [67]. We thus concluded that CO dissociation is mainly in the direct route on Fe_5C_2(510).

In the *ha*-SiO_2/Fe_5C_2(510) case, the originally preferred $\mathbf{4F_1}$-site for the dissociated C from CO at the **T**-site is occupied by the interface silica, thus hindering the T-site CO dissociation. Alternatively, the CO on the interface of *ha*-SiO_2/Fe_5C_2(510) is stably located at the interface $\mathbf{3F_4}$-site with the E_b value –2.12 eV, as shown in Fig. S3 (b) of the SI, which is more negative than that –1.95 eV at the similar **3F** site on Fe_5C_2(510). The result shows that the CO molecule binds more strongly to the interface Fe atom in the *ha*-SiO_2/Fe_5C_2(510) case than that in the Fe_5C_2(510) case; It is reasonable because the distance between the H atom of the interface SiO—H and the O atom of the CO molecule is 2.47 Å, indicating the hydrogen bond interaction. The energy profile of the $\mathbf{3F_4}$-site CO dissociation, as given in Figs. 3(b) and S4 (b) of the SI, indicates that the H-assisted CO dissociation via the HCO intermediate overcomes the E_a 1.39 eV to form the HCO intermediate with an endothermicity of 0.85 eV and continues to surpass an E_a 0.99 eV for breaking the C—O bond of the HCO intermediate. Additionally, the O-end hydrogenation is difficult because the adsorption geometry of CO molecule is in vertical orientation to the surface like the case in the Fe_5C_2(510)

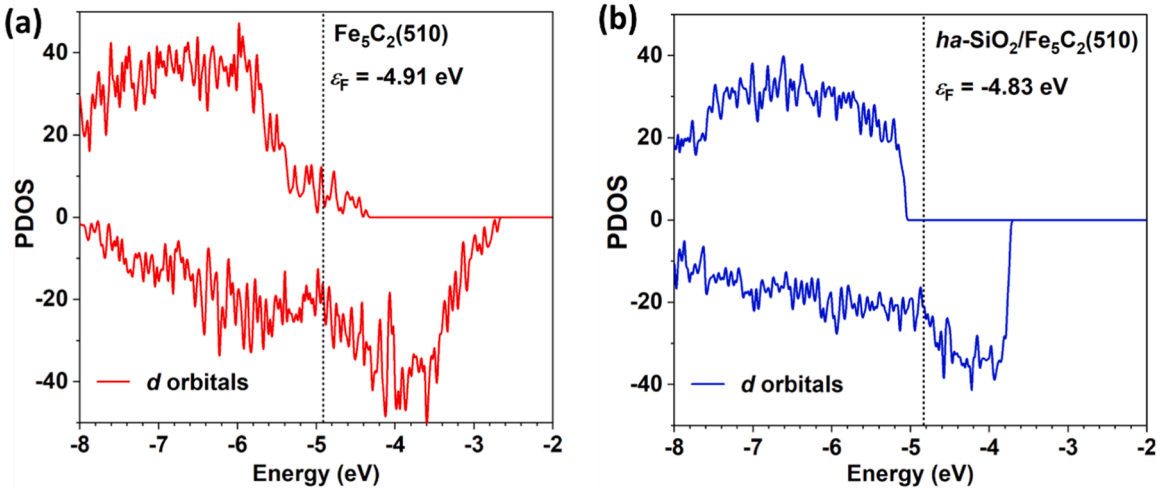

Fig. 2. The PDOSs of the top-layer Fe and C atoms in Fe_5C_2(510) (a) and *ha*-SiO_2/Fe_5C_2(510) (b), respectively.

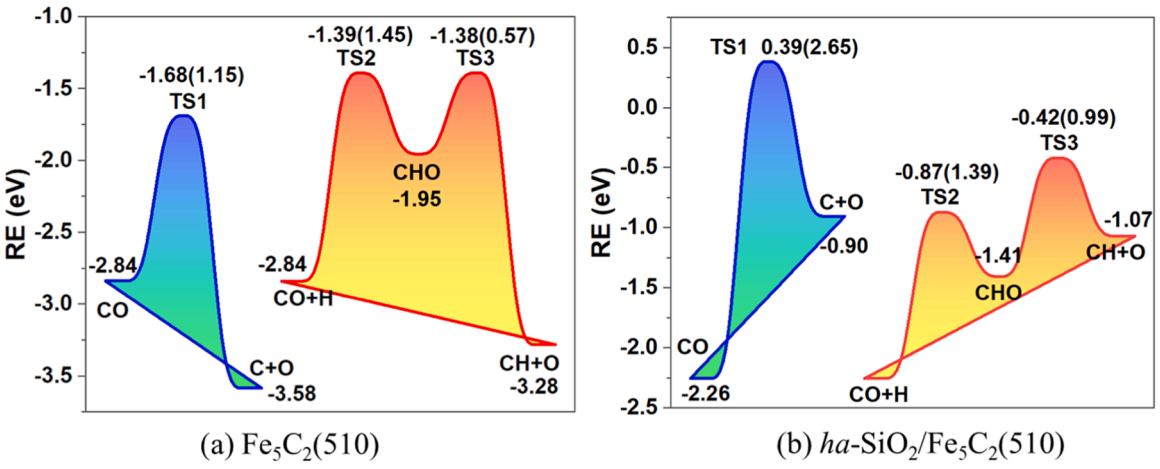

Fig. 3. Energy profiles for CO dissociation on Fe_5C_2(510) (a) and *ha*-SiO_2/Fe_5C_2(510) (b). The energy in the blank is the activation barrier.

case. Thus, the E_a value (1.84 eV) for the H-assisted CO dissociation is smaller than that for CO direct dissociation (2.65 eV). The result suggests that on the interface of *ha*-SiO_2/Fe_5C_2(510), the H-assisted route via the HCO intermediate is easier than the CO direct dissociation, but is more difficult than the CO dissociation on the clean surface of Fe_5C_2(510). We therefore concluded that the H-assisted CO dissociation occurs on the interface of *ha*-SiO_2/Fe_5C_2(510).

The above results show that CO dissociation becomes difficult as the cases going from Fe_5C_2(510) to *ha*-SiO_2/Fe_5C_2(510) and we explained the reason(s) why as follows. Even for the **3F**-site CO on Fe_5C_2(510), the E_b value is just less negative than that of the **T**-site CO (by 0.18 eV), which is still much smaller than the increase for the E_a value of CO direct dissociation (by 1.50 eV), suggesting that the inaccessibility of the originally preferred **4F$_1$**-site for the CO dissociation is not the main reason. Before CO adsorption, the CO-bonded two Fe atoms have the positive charges increased from 1.00 *e* to 1.02 *e* as the cases going from Fe_5C_2(510) to *ha*-SiO_2/Fe_5C_2(510), which does not favor CO activation. In another perspective, CO dissociation is regarded as the oxidative addition of CO to Fe. There occurs charge transfer by 2.40 *e* from the surface Fe to the ligand SiO_2 and lowers the $\varepsilon_{dc\text{-}VB}$ value of Fe from 7.26 eV to 7.28 eV, which does not favor the oxidative addition of CO to Fe, because the oxidative addition usually gets difficult when the valence orbital energy of metal catalysts is lowered.

3.3. CH_4 formation

Methane is an undesired but inevitable product of the FTS. CH_4 formation contains multi-step elementary reactions in experiment, which could happen through the step-wised hydrogenations by the surface C and the additional C from CO dissociation. Methanation energy profiles for the surface C and the additional C on Fe_5C_2(510) and *ha*-SiO_2/Fe_5C_2 (510) were discussed below.

In the Fe_5C_2(510) case, there are two kinds of the upmost C atoms, respectively at the Fe-rich region and Fe-poor region (Fig. S5 of the SI). The two kinds of C atoms have the similar Bader charges (–1.08 *e* and –1.04 *e*), the similar activation barriers ($E_{a\_eff,CH4}$) of CH_4 formation (3.58 eV and 3.51 eV), and the similar increasing trends of total energy in the reaction coordinate, where the lowest energy point is by the H adsorption around the C atom and the highest energy point is by the transition state (TS) for the final hydrogenation (Fig. S5 of the SI). Herein, we mainly discussed the methanation of the upmost C atom at the Fe-rich region, marked by C^O in Fig. 4(a), because the H element prefers the Fe-rich region more than the Fe-poor region. An additional C (marked by C^A) from CO dissociation is left at the **4F**-site and its methanation is further employed. CH_4 formation processes of C^O and C^A (marked by R_C^O and R_C^A, respectively) on Fe_5C_2(510) are presented by Fig. 4(b), with the TS structures for each hydrogenation step given in Fig. S6 of the SI and detailed energy parameters shown in Table S3 of the SI. The C^A adsorption causes the H adsorption energy changed from

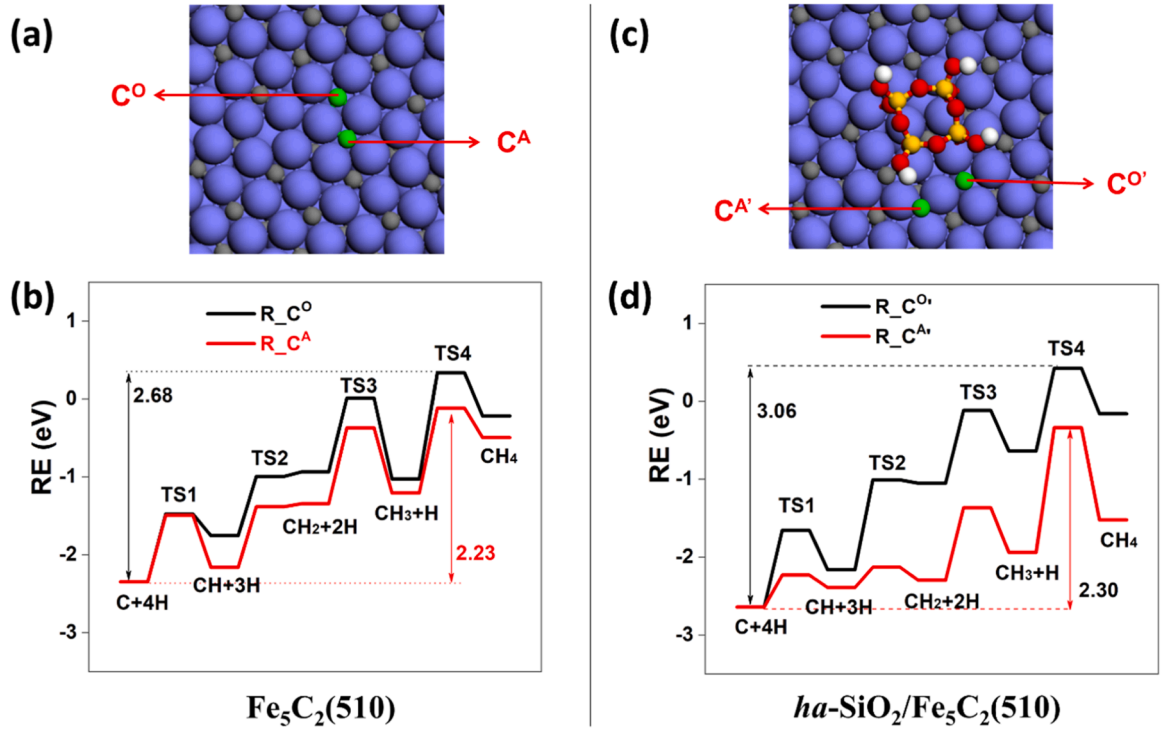

Fig. 4. The original surface C atom (C^O) and the additional C atom (C^A) (a) and energy profiles of CH_4 formation by the C^O hydrogenation (R_C^O) and C^A hydrogenation (R_C^A) on Fe_5C_2(510) (b). The original surface C atom ($C^{O\prime}$) and the additional C atom ($C^{A\prime}$) (c) and energy profiles of CH_4 formation by the $C^{O\prime}$ hydrogenation ($R\_C^{O\prime}$) and C^A hydrogenation ($R\_C^{A\prime}$) on *ha*-SiO_2/Fe_5C_2 (510) (d).

–0.71 eV to –0.59 eV. On routes of R_C^O and R_C^A, similar increasing tendencies of hydrogenation coordinate were found for the hydrogenation TSs with the highest total energy at the TS4. Accordingly, the $E_{a\_eff,CH4}$ value is the *RE* difference between the surface C + 4H and the TS4 of CH_3 hydrogenation. The C^A compared to the C^O has a lower $E_{a\_eff,CH4}$ (2.23 eV and 2.68 eV, respectively). Thus, we concluded that the CH_4 formation by the C^A hydrogenations is easier than the C^O hydrogenations.

In the case of *ha*-SiO_2/Fe_5C_2(510), the existence of 4-membered *ha*-SiO_2 makes the interface C in different coordination environment. In the *ha*-SiO_2/Fe_5C_2(510) case, three kinds of interface C atoms, marked by $C^{O\prime}$–1, $C^{O\prime}$–2, and $C^{O\prime}$–3, are close to Fe–O–Si bonds, as shown in Fig. S7 of the SI. The interface C^0–1 is close to one **2F**-site O atom; the interface C^0–2 is close to one **2F**-site O atom and one **3F**-site O atom; the interface C^0–3 is close to two **3F**-site O atoms. The $C^{O\prime}$–1, $C^{O\prime}$–2, and $C^{O\prime}$–3 atoms are charged by –1.04 *e*, –1.01 *e*, and –1.07 *e*, respectively, and are less negative than the charge –1.08 *e* for the surface C at the Fe-rich region on Fe_5C_2(510) because of the charge transfer from the surface Fe to the *ha*-SiO_2 ligand. Around the $C^{O\prime}$–1, $C^{O\prime}$–2, and $C^{O\prime}$–3, the most stable H atom are located at nearby $\mathbf{3F_1}$, $\mathbf{3F_2}$, and $\mathbf{3F_3}$ sites, respectively with E_b values of –0.70 eV, –0.68 eV, and –0.54 eV. Energy profiles (Fig. S7, the TS structures in Fig. S8, and energy parameters in Table S3 of the SI) of methanation for the interface $C^{O\prime}$–1, $C^{O\prime}$–2, and $C^{O\prime}$–3 are shown by $R\_C^{O\prime}$–1, $R\_C^{O\prime}$–2, and $R\_C^{O\prime}$–3, respectively. CH_4 formation by the route $R\_C^{O\prime}$–1 has the $E_{a\_eff,CH4}$ of 3.26 eV, higher than those of 3.07 eV and 3.00 eV, respectively by the routes $R\_C^{O\prime}$–2 and $R\_C^{O\prime}$–3. Because the route $R\_C^{O\prime}$–2 has advantages in stability of the adsorbed H, intermediates of CH and CH_2, and the four TSs, the interface $C^{O\prime}$–2 is relatively easier to be mechanized. Therefore, the adsorption sites for an additional C (marked by $C^{A\prime}$) is mainly confined around the interface C-2 (newly marked by $C^{O\prime}$) in Fig. 4(c). The additional $C^{A\prime}$ located at the $\mathbf{3F_4}$-site around the $C^{O\prime}$ atom is stable, as shown by Fig. S3 (c) of the SI. Methanation energy profiles for $C^{O\prime}$ ($R\_C^{O\prime}$) and $C^{A\prime}$ ($R\_C^{A\prime}$) are shown in Fig. 4(d) with the corresponding TS structures in Fig. S9 and energy parameters in Table S3 of the SI. The $R\_C^{A\prime}$ compared to the $R\_C^{O\prime}$ has the lower $E_{a\_eff,CH4}$ (2.30 eV vs. 3.07 eV), which was ascribed to the less steric hindrance from interface *ha*-SiO_2 for the H attacking in the methanation process confirmed by the more stable intermediates and lower TS energies on the $R\_C^{A\prime}$. These results showed that CH_4 formation by the additional $C^{A\prime}$ hydrogenations are easier than that by the interface $C^{O\prime}$ hydrogenations.

3.4. C_2 formation

Ability of C_2 formation was compared in between the Fe_5C_2(510) and *ha*-SiO_2/Fe_5C_2(510) cases by investigating $C_1 + C_1$ coupling following carbide ($CH_i + CH_j \rightarrow CH_iCH_j$, i and $j = 0 \sim 3$) and CO-insertion ($CO + CH_j \rightarrow COCH_j$, $j = 0 \sim 3$) mechanisms. $C_1 + C_1$ coupling was calculated for the surface C^O and adsorbed C^A in Fig. 4(a) and the surface $C^{O\prime}$ and adsorbed $C^{A\prime}$ in Fig. 4(c); the superscripts "O" and "A" are used to denote the C is the original atom in the surface and the additional atom from CO dissociation, respectively; the superscripts "′" is used to distinguish the *ha*-SiO_2/Fe_5C_2(510) case from the Fe_5C_2(510) case. Because hydrogenation is much easier by C^A (or $C^{A\prime}$) than that by C^O (or $C^{O\prime}$), as suggested by Fig. 4, the CH_i+ CH_j coupling in the $i \leq j$ case was calculated as $C^OH_i + C^AH_j$ (or $C^{O\prime}H_i + C^{A\prime}H_j$). With the reference of three gaseous H_2 molecules, energy profiles of C_2 formation were presented in Fig. 5. The corresponding structures about the IS, TS, and FS, together with the E_a and E_r values were given in Figs. S10 and S11 of the SI. On the energy profiles, the highest TS energy for CH_4 formation was also calibrated for comparison convenience.

From the energy profiles in Fig. 5(a), the CCH, CHCH and CCO species are found to be more stable than other C_2 species in thermodynamics on the surface of Fe_5C_2(510). In kinetics, the carbide mechanisms involved with CH_2 and CH_3 have the higher effective barriers than that of 2.23 eV for CH_4 formation, because of the energetic instability of CH_2 and CH_3 as well as the steric repulsion between H-rich C_1 intermediates [69]. Thus, CH_2 and CH_3 are not active species for carbon chain growth on this surface. The C + C, C + CH, and CH + CH couplings have lower effective barriers than that of 2.23 eV for CH_4 formation,

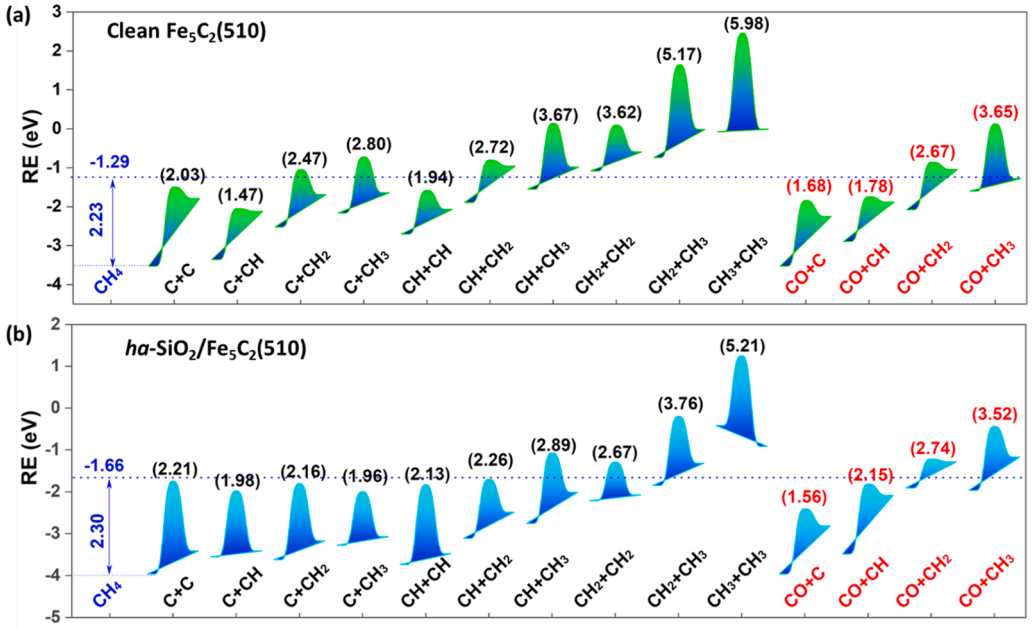

Fig. 5. Energy profiles for C_1 + C_1 coupling on Fe_5C_2(510) (a) and *ha*-SiO_2/Fe_5C_2 (510) (b). Number in parentheses denotes as the effective barrier of coupling reactions.

suggesting that these couplings might be the major coupling pathways. The C + CH coupling with the lowest effective barrier of 1.47 eV is regarded as the most feasible carbide mechanism, which is in agreement with the literature report [46]. CO-inserted mechanisms by CH_2 + CO and CH_3 + CO couplings have higher effective barriers, and the C + CO and CH + CO couplings have the lower effective barriers than that of 2.23 eV for CH_4 formation. The CHO species produced by the CO hydrogenation in the H-assisted CO dissociation also might take part in C_1 + C_1 coupling but the process hardly occurs due to thermodynamic instability implied by the high energy in energy profiles of CO dissociation. One should aware that the CO-inserted mechanism is in competition with CO dissociation. The lower barrier for CO dissociation compared to the C + CO coupling means that the C–O bond could have been broken before the CO-inserted mechanism (1.15 eV vs. 1.68 eV). Therefore, it can be concluded that the CO-inserted mechanism is infeasible and less C_2 oxygenate will be produced on the clean Fe_5C_2(510) surface.

On the interface of *ha*-SiO_2/Fe_5C_2(510), as shown in Fig. 5(b), the CC, CCH, CCH_2, CCH_3, CHCH, and CCO exhibit energetic advantages over other C_2 species. The couplings with CH_2 and CH_3, excluding the C + CH_2 and C + CH_3 couplings, are difficult to occur because of higher effective barriers. The effective barriers for carbide routes by C + C, C + CH, C + CH_2, C + CH_3, CH + CH, and CH + CH_2 couplings are lower than that of 2.30 eV for CH_4 formation, and get the minimum of 1.96 eV by the C + CH_3 coupling. Therefore, the C + CH_3 coupling is the most feasible carbide mechanism. CO-inserted mechanisms could be facilitated on the ground that CO dissociation is difficult on the interface of *ha*-SiO_2/Fe_5C_2(510). Among the CO-inserted routes, the C + CO coupling has the lowest effective barrier of 1.58 eV, making it more accessible than other CO-inserted routes. Considering the energetic advantage of the HCO intermediate in the process of CO dissociation, the coupling with HCO is also considered but hardly occurs, as demonstrated by the C + CHO coupling with a higher effective energy (3.26 eV) than that for CH_4 formation, as shown in Fig. 6. Because both the CH_i hydrogenation and CO hydrogenation need too much energy, the CH_i+ CHO coupling is not so favorable as the C + CO coupling. The C + CO coupling has lower barriers than the most possible direct route for CO dissociation (1.56 eV vs. 2.78 eV, respectively). Also, cleavage of C—O bond in the CCO is difficult with the high effective barrier (3.27 eV). The

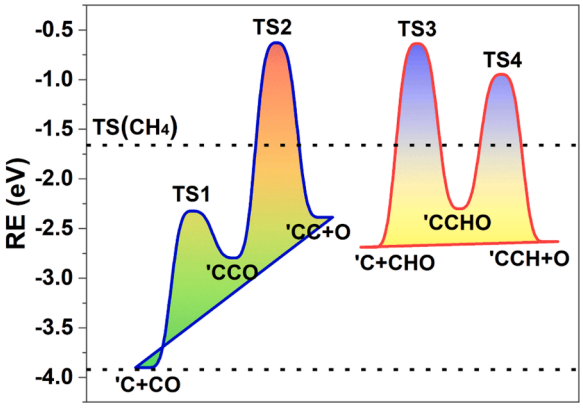

Fig. 6. Energy profiles of the C—O bond breaking after the C + CO coupling and the C+CHO coupling on the interface of *ha*-SiO_2/Fe_5C_2(510) where 'C is singed for interface C.

results imply that the C—O bond is difficult to activate on the interface of *ha*-SiO_2/Fe_5C_2(510) either by direct and H-assisted CO dissociation or after coupling with interface C_1 species. As such, this interface facilitates C + CO coupling as the most feasible pathway for C_1 + C_1 coupling with the CCO as one important C_2 oxygenate.

Above results showed that on the Fe_5C_2(510) surface, the most feasible carbide mechanism occurring by the C + CH coupling has the effective barrier (1.47 eV) lower than that of the most feasible CO-inserted mechanism occurring by the C + CO coupling (1.68 eV), by 0.21 eV. At the interface of *ha*-SiO_2/Fe_5C_2(510), the most feasible carbide mechanism occurring also by the C + CH coupling has the effective barrier (1.98 eV) higher than that of the most feasible CO-inserted mechanism occurring by the C + CO coupling (1.56 eV), by 0.42 eV. Thus, we concluded that the reaction pathway is shifted from the carbide mechanism (the C + CH coupling) to the CO-inserted mechanism (the C + CO coupling) after silica modification.

To understand the reason(s) for the shift in the reaction pathway after silica modification, it is necessary to make it clear that why the effective barrier is increased for the C + CH coupling (by 0.51 eV from

1.47 eV to 1.98 eV) and decreased for the C + CO coupling (by 0.12 eV from 1.68 eV to 1.56 eV). When the case goes from the $Fe_5C_2(510)$ surface to the *ha*-$SiO_2/Fe_5C_2(510)$ interface, the decrease of the effective barrier for the C + CO coupling is contributed mainly by the destabilization of CO adsorption (by 0.10 eV). The next is to find the reason(s) for the increase of the effective barrier for the C + CH coupling after silica modification.

We divided the model into two moieties and made interaction-deformation energies analysis, as shown in Fig. 7. The first is the C + CH moiety just consisting of the C and CH species, the second is the rest moiety except the C + CH moiety. We make analysis for the changes of the interaction energy between the C and CH species in the first moiety (ΔE_{int1} and $\Delta E'_{int1}$), the interaction energy between the two moieties (ΔE_{int2} and $\Delta E'_{int2}$), and the deformation energy of the second moiety (E_{def} and E'_{def}) from the IS to the TS; In these terms, the superscribe "′" means the case in the *ha*-$SiO_2/Fe_5C_2(510)$ interface is used to distinguish from the case in the $Fe_5C_2(510)$ surface and the computational details are given in the Page S15 of the SI. And then, the difference between these terms ($\Delta\Delta E_{int1} = \Delta E'_{int1} - \Delta E_{int1}$; $\Delta\Delta E_{int2} = \Delta E'_{int2} - \Delta E_{int2}$; $\Delta E_{def} = E'_{def} - E_{def}$) from the $Fe_5C_2(510)$ surface to the *ha*-$SiO_2/Fe_5C_2(510)$ interface are calculated to find the influence(s) of silica modification.

As going from the $Fe_5C_2(510)$ surface to the *ha*-$SiO_2/Fe_5C_2(510)$ interface, the difference between the interaction energies between the C and CH species gets weaker by 1.38 eV ($\Delta\Delta E_{int1}$); This change makes the TS less stable in the *ha*-$SiO_2/Fe_5C_2(510)$ case than in the $Fe_5C_2(510)$ case. However, the difference between the interaction energy between the two moieties ($\Delta\Delta E_{int2}$) becomes more negative by 0.12 eV and the difference between the deformation energies of the second moiety (ΔE_{def}) gets smaller by 0.29 eV; These two changes make the TS more stable in the *ha*-$SiO_2/Fe_5C_2(510)$ case than that in the $Fe_5C_2(510)$ case. These results strongly indicated that the weak interaction between the C and CH species is suppressed after silica modification and responsible for the greatly increased effective barrier by 0.51 eV. As going from the $Fe_5C_2(510)$ surface to the *ha*-$SiO_2/Fe_5C_2(510)$ interface, the distance between the C and CH species $d_{(C—C)}$ becomes longer by 0.265 Å (from 1.723 Å to 1.988 Å), which agrees well with results that the interaction between the C and CH species is weakened and the interaction between the two moieties are strengthened. The distance between the Fe2 and Fe5 atoms directly binding with the C and CH species considerably gets shorter by 0.481 Å (from 3.005 Å to 2.514 Å), which agrees well with the result that the interaction between the C and CH species gets weaker, suggesting that the silica modification suppresses the deformation of the surface caused by the forming C—CH bond from the IS to the TS and therefore the C + CH coupling becomes difficult when the case changes from the $Fe_5C_2(510)$ surface to the interface of *ha*-$SiO_2/Fe_5C_2(510)$.

The above analysis shows that the silica modification suppresses both the deformation of the surface caused by the forming C—C bond in the carbide mechanism and the C—O bond cleavage in the CO-inserted mechanism, thus resulting in the shifting of the reaction pathway from the carbide mechanism (the C + CH coupling) to the CO-inserted mechanism (the C + CO coupling) after silica modification.

3.5. Selectivity of CH_4 and C_2 oxygenate

In order to assess the selectivity of CH_4 and C_2 species in FTS, few well-accepted assumptions according to literatures was made as follows [70–75] With steady-state approximations, the reactions prior to the hydrogenation of CH_3 are in quasi-equilibrium and the hydrogenation of CH_3 with the highest energy of TS is the rate-determined step for CH_4 formation. Our calculation results of CH_4 formation and $C_1 + C_1$ coupling show that the CH_x hydrogenation is easier than the C—C bond formation by either the carbide mechanism or the CO-inserted mechanism. Under typical FT reaction conditions, the $C_1 + C_1$ coupling reactions are usually considered to be irreversible, desorption of the hydrogenated hydrocarbon is the rate-determining step, and thus the hydrogenation reactions are in quasi-equilibrium at steady-state prior to hydrocarbon desorption. On the basis of these assumptions and following micro-kinetics proposed by Hu group[70,76] and widely used in literatures [46,54,77,78], the larger positive value of $\Delta E_{a\_eff} = E_{a\_eff,CH4} - E_{a\_eff,C1+C1}$ means that C_2 formation occurs more easily, where the terms $E_{a\_eff,CH4}$ and $E_{a\_eff,C1+C1}$ are the effective barriers for the formations of CH_4 and C_2 species, respectively; More details of the micro-kinetics on CH_4 formation and $C_1 + C_1$ coupling are given in the Page S17 of the SI.

$C_1 + C_1$ coupling in the $Fe_5C_2(510)$ case mainly follows the carbide route of C + CH coupling and in the *ha*-$SiO_2/Fe_5C_2(510)$ case mainly

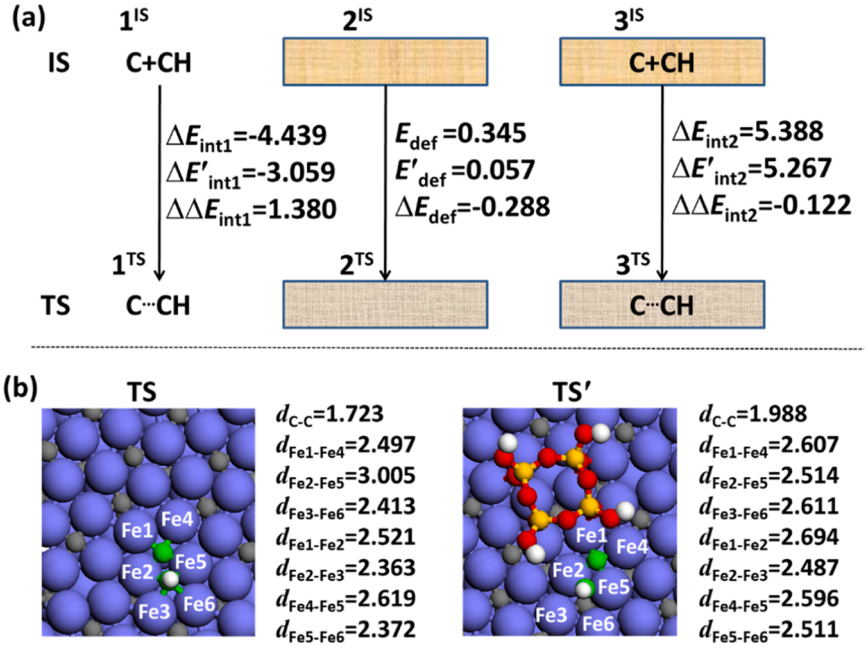

Fig. 7. The change of interaction energies between the C + CH moiety and the rest moiety as going from the $Fe_5C_2(510)$ surface to the *ha*-$SiO_2/Fe_5C_2(510)$ interface and the geometry parameters of the transition state (TS) in the $Fe_5C_2(510)$ case and TS′ in the *ha*-$SiO_2/Fe_5C_2(510)$ case. All the energies are in eV and the distances are in Å.

follows CO-inserted route of C + CO coupling. Based on the most feasible coupling, the ΔE_{a_eff} value in the *ha*-SiO_2/Fe_5C_2(510) case is just smaller by 0.01 eV than that in the Fe_5C_2(510) case, indicating the similar selectivity of CH_4 to C_2 in the two cases. On the Fe_5C_2(510) surface, CO-inserted mechanisms are nearly infeasible for $C_1 + C_1$ coupling because CO dissociation is easy, and thus the main C_2 product is O-excluded. On the *ha*-SiO_2/Fe_5C_2(510) interface, $C_1 + C_1$ coupling can follow the CO-inserted route, indicating that the main C_2 product is O-contained. Compared to the Fe_5C_2(510) case, the C_2 oxygenate selectivity is enhanced in the *ha*-SiO_2/Fe_5C_2(510) case. From the viewpoint of structural properties, the *ha*-SiO_2 ligand covers the active site and anchors CO at the inactive site via the hydrogen bond, thus hindering the CO dissociation but promoting the CO-inserted mechanism. From the viewpoint of electronic properties, the *d*-valence band center lowers in energy when the Fe_5C_2(510) surface is modified with the *ha*-SiO_2 ligand, which does not favor the C–O bond cleavage for both CO molecule and CCO species, because usually the oxidative addition is suppressed when the *d* orbital of metal catalysts exists at a low energy and the C–O bond cleavage is understood to be oxidative addition. The result is in agreement with the experimental result that the selectivity of C_2 oxygenates is higher for the iron catalysts modified with silica in w/o micro-emulsions than that for the impregnated catalysts [43]. However, the reactive sites provided by the iron carbide are generally more active than those sites close to the silica species in terms of the FTS activity and in the most cases the carbide mechanism remains the main route for carbon chain growth for the whole catalyst of iron carbide after silica modification. Our results could enrich the knowledge of the intrinsic catalytic role(s) of the interface between the iron carbide catalysts and the support of silica in the FTS.

4. Conclusion

In this work, we theoretically investigated surface modification of Fe_5C_2 by silica-based ligand and its influence on C_2 oxygenate selectivity in the Fischer-Tropsch Synthesis by carrying out a theoretical study of CO dissociation, CH_4 formation and $C_1 + C_1$ coupling on the Fe_5C_2(510) surface and the *ha*-SiO_2/Fe_5C_2(510) interface. The inversed model of *ha*-SiO_2/Fe_5C_2(510) is constructed by assuming the dehydration-dehydrogenation reaction occurring between the $Si(OH)_4$ gas molecules and the Fe_5C_2(510) surface with the formation of Fe–O–Si bonds on the interface.

It was found that CO dissociation on the clean model is easier by the direct route than that by the H-assisted route. CH_4 formation was calculated for the upmost C and the additional C from CO dissociation on two modes of the clean surface of Fe_5C_2(510) and the interface of *ha*-SiO_2/Fe_5C_2(510). On the two modes, the additional C is easier to be hydrogenated into CH_4 than the upmost C. The $C_1 + C_1$ coupling proceeds by the carbide mechanism with C + CH coupling as the most feasible route instead of the CO-inserted mechanisms because CO dissociation is easy.

On the interface of *ha*-SiO_2/Fe_5C_2(510), the CO dissociation becomes difficult because the *d*-valence band center decreases when binding with the *ha*-SiO_2 ligand. The *ha*-SiO_2 anchors CO via the hydrogen bond, which hinders the CO dissociation but facilitates the CO coupling with interface C. Meanwhile, the silica modification suppresses the deformation of the surface caused by the forming C—CH bond from the IS to the TS and thus the C + CH coupling becomes difficult when the case changes from the surface of Fe_5C_2(510) to the interface of *ha*-SiO_2/Fe_5C_2(510). Therefore, the interface changes the main pathway of $C_1 + C_1$ coupling into the CO-inserted mechanism with formation of C_2 oxygenates as the cases going from the clean surface of Fe_5C_2(510) to the interface of *ha*-SiO_2/Fe_5C_2(510). The similar selectivity of CH_4 and higher selectivity of CCO on the *ha*-SiO_2/Fe_5C_2(510) interface were concluded by comparing the effective barrier difference between CH_4 formation and $C_1 + C_1$ coupling to that on the clean surface of Fe_5C_2(510). The enhanced selectivity of C_2 oxygenates was ascribed to the reduced reactivity of the C + CH coupling and the C—O bond cleavage. Note that the reactive sites provided by the iron carbide are generally responsible for the FTS activity and in the most cases the carbide mechanism remains the main route for carbon chain growth for the whole catalyst of iron carbide after silica modification. Our results provided some helpful insights for understanding the influence on catalytic selectively by surface modification of silica ligand on the silica-supported iron carbide catalysts in the FTS.

Influence of the slab thickness on coupling reactions on Fe_5C_2(510) (Table S1); parameters about the silica rings on Fe_5C_2(510) (Table S2); energy parameters about CH_4 formation on the clean surface and the interface (Table S3); inversed modes and energies of interface structures (Fig. S1); the stability of the interface structure under the reaction temperature (Fig. S2); adsorption of C and CO on the interface (Fig. S3); Geometry changes of the CO dissociation (Fig. S4); methanation energy profiles and adsorption structures of the H atom, intermediates, and TS along the coordinate of CH_4 formation on the clean surface and the interface (Figs. S5 ~ S9); energies and structures for $C_1 + C_1$ couplings on the clean surface and the interface (Figs. S10 and S11). Interaction-deformation energies analysis; Microkinetic analyses.

CRediT authorship contribution statement

Junqing Yin: Conceptualization, Data curation, Investigation, Visualization, Formal analysis, Methodology, Validation, Writing – original draft, Writing – review & editing, Project administration, Resources, Supervision, Funding acquisition. **Shuyuan Wang:** Conceptualization, Writing – review & editing, Funding acquisition. **Dan Xu:** Conceptualization, Writing – review & editing. **Yong You:** Writing – review & editing. **Xingchen Liu:** Conceptualization, Methodology, Software, Writing – review & editing. **Qing Peng:** Conceptualization, Methodology, Software, Writing – review & editing.

Declaration of Competing Interest

The authors declare that they have no known competing financial interests or personal relationships that could have appeared to influence the work reported in this paper.

Data availability

Data will be made available on request.

Acknowledgments

The authors are grateful for the Natural Science Foundation of Sichuan Province (No. 2023NSFSC1080), the Talent Program of Chengdu University (No. 2081923010), Qilu University of Technology (Shandong Academy of Sciences) Project (NO. 2022JBZ02–03), and the funding support from Synfuels China Co. Ltd.

Supplementary materials

Supplementary material associated with this article can be found, in the online version, at doi:10.1016/j.mcat.2023.113333.

References

[1] S.J. Tauster, S.C. Fung, Strong metal-support interactions: occurrence among the binary oxides of groups IIA–VB, J. Catal. 55 (1978) 29–35.
[2] S.J. Tauster, S.C. Fung, R.T.K. Baker, J.A. Horsley, Strong interactions in supported-metal catalysts, Science 211 (1981) 1121–1125.
[3] H. Praliaud, G.A. Martin, Evidence of a strong metal-support interaction and of Ni-Si alloy formation in silica-supported nickel catalysts, J. Catal. 72 (1981) 394–396.
[4] D. Kim, N. Becknell, Y. Yu, P.D. Yang, Room-temperature dynamics of vanishing copper nanoparticles supported on silica, Nano Lett. 17 (2017) 2732–2737.

[5] S. Zhang, P.N. Plessow, J.J. Willis, S. Dai, M.J. Xu, G.W. Graham, M. Cargnello, F. Abild-Pedersen, X.Q. Pan, Dynamical observation and detailed description of catalysts under strong metal–support interaction, Nano Lett. 16 (2016) 4528–4534.

[6] Y. Lykhach, S.M. Kozlov, T. Skála, A. Tovt, V. Stetsovych, N. Tsud, F. Dvořák, V. Johánek, A. Neitzel, J. Mysliveček, Counting electrons on supported nanoparticles, Nat. Mater. 15 (2016) 284–288.

[7] D.J. Duvenhage, R.L. Espinoza, N.J. Coville, Fischer-Tropsch precipitated iron catalysts: deactivation studies, Surf. Sci. Catal. 88 (1994) 351–358.

[8] W. Ning, N. Koizumi, H. Chang, T. Mochizuki, T. Itoh, M. Yamada, Phase transformation of unpromoted and promoted Fe catalysts and the formation of carbonaceous compounds during Fischer–Tropsch synthesis reaction, Appl. Catal. A-Gen. 312 (2006) 35–44.

[9] N.S. Govender, M.J.V. Vuuren, M. Claeys, E. van Steen, Importance of the usage ratio in iron-based Fischer−Tropsch synthesis with recycle, Ind. Eng. Chem. Res. 45 (2006) 8629–8633.

[10] R. Zhao, K. Sudsakorn, J.G. Goodwin, K. Jothimurugesan, S.K. Gangwal, J. J. Spivey, Attrition resistance of spray-dried iron F–T catalysts: effect of activation conditions, Catal. Today 71 (2002) 319–326.

[11] K. Sudsakorn, J.G. Goodwin, A.A. Adeyiga, Effect of activation method on Fe FTS catalysts: investigation at the site level using SSITKA, J. Catal. 213 (2003) 204–210.

[12] H.M.T. Galvis, J.H. Bitter, T. Davidian, M. Ruitenbeek, A.I. Dugulan, K.P. de Jong, Iron particle size effects for direct production of lower olefins from synthesis gas, J. Am. Chem. Soc. 134 (2012) 16207–16215.

[13] A.N. Pour, M.R. Housaindokht, M. Irani, S.M.K. Shahri, Size-dependent studies of Fischer–Tropsch synthesis on iron based catalyst: new kinetic model, Fuel 116 (2014) 787–793.

[14] T.A. Wezendonk, V.P. Santos, M.A. Nasalevich, Q.S.E. Warringa, A.I. Dugulan, A. Chojecki, A.C.J. Koeken, M. Ruitenbeek, G. Meima, H.U. Islam, G. Sankar, M. Makkee, F. Kapteijn, J. Gascon, Elucidating the nature of Fe species during pyrolysis of the Fe-BTC MOF into highly active and stable Fischer–Tropsch catalysts, ACS Catal. 6 (2016) 3236–3247.

[15] T.A. Wezendonk, X.H. Sun, A.I. Dugulan, A.J.F. van Hoof, E.J.M. Hensen, F. Kapteijn, J. Gascon, Controlled formation of iron carbides and their performance in Fischer-Tropsch synthesis, J. Catal. 362 (2018) 106–117.

[16] J. Wang, S. Huang, S. Howard, B.W. Muir, H. Wang, D.F. Kennedy, X. Ma, Elucidating surface and bulk phase transformation in Fischer–Tropsch synthesis catalysts and their influences on catalytic performance, ACS Catal. 9 (2019) 7976–7983.

[17] H. Xiong, M.A. Motchelaho, M. Moyo, L.L. Jewell, N.J. Coville, Effect of Group I alkali metal promoters on Fe/CNT catalysts in Fischer–Tropsch synthesis, Fuel 150 (2015) 687–696.

[18] P. Zhai, C. Xu, R. Gao, X. Liu, M. Li, W. Li, X. Fu, C. Jia, J. Xie, M. Zhao, X. Wang, Y. W. Li, Q. Zhang, X.D. Wen, D. Ma, Highly tunable selectivity for syngas-derived alkenes over Zinc and Sodium-modulated Fe5C2 catalyst, Angew. Chem. Int. Ed. 55 (2016) 1–7.

[19] H.M.T. Galvis, J.H. Bitter, C.B. Khare, M. Ruitenbeek, A.I. Dugulan, K.P. de Jong, Supported iron nanoparticles as catalysts for sustainable production of lower olefins, Science 315 (2012) 835–838.

[20] G.B. Raupp, W.N. Delgass, Mössbauer investigation of supported Fe catalysts: III. In situ kinetics and spectroscopy during Fischer-Tropsch synthesis, J. Catal. 58 (1979) 361–369.

[21] M.E. Dry, The Fischer-Tropsch-synthesis in catalysis, Catal. Sci. Technol. 1 (1981) 159–255.

[22] H.J. Wan, B.S. Wu, H.W. Xiang, Y.W. Li, Fischer–Tropsch synthesis: influence of support incorporation manner on metal dispersion, metal–support interaction, and activities of iron catalysts, ACS. Catal. 2 (2012) 1877–1883.

[23] N.O. Egiebor, W.C. Cooper, Fischer-tropsch synthesis on a precipitated iron catalyst: influence of silica support on product selectivities, Can. J. Chem. Eng. 63 (1985) 81–85.

[24] C.H. Zhang, H.J. Wan, Y. Yang, H.W. Xiang, Y.W. Li, Study on the iron–silica interaction of a co-precipitated Fe/SiO_2 Fischer–Tropsch synthesis catalyst, Catal. Commun. 7 (2006) 733–738.

[25] H.J. Wan, B.S. Wu, Z.C. Tao, T.Z. Li, X. An, H.W. Xiang, Y.W. Li, Study of an iron-based Fischer–Tropsch synthesis catalyst incorporated with SiO_2, J. Mol. Catal. A-Chem. 260 (2006) 255–263.

[26] H.Y. Suo, S.G. Wang, C.H. Zhang, J. Xu, B.S. Wu, Y. Yong, H.W. Xiang, Y.W. Li, Chemical and structural effects of silica in iron-based Fischer–Tropsch synthesis catalysts, J. Catal. 286 (2012) 111–123.

[27] A.F.H. Wielers, A.J.H.M. Kock, C.E.C.A. Hop, J.W. Geus, A.M. van Der Kraan, The reduction behavior of silica-supported and alumina-supported iron catalysts: a Mössbauer and infrared spectroscopic study, J. Catal. 117 (1989) 1–18.

[28] A.J.H.M. Kock, H.M. Fortuin, J.W. Geus, The reduction behavior of supported iron catalysts in hydrogen or carbon monoxide atmospheres, J. Catal. 96 (1985) 261–275.

[29] X. Zhou, G.J.A. Mannie, J. Yin, X. Yu, C.J. Weststrate, X.D. Wen, K. Wu, Y. Yang, Y. W. Li, J.W. Niemantsverdriet, Iron carbidization on thin-film silica and silicon: a near-ambient-pressure X-ray photoelectron spectroscopy and scanning tunneling microscopy study, ACS Catal 8 (2018) 7326–7333.

[30] C.A. Bradley, M.J. McMurdo, T.D. Tilley, Selective catalytic cyclohexene oxidation using titanium-functionalized silicone nanospheres, J. Phys. Chem. C 111 (2007) 17570–17579.

[31] F. Novio, D. Monahan, Y. Coppel, G. Antorrena, P. Lecante, K. Philippot, B. Chaudret, Surface chemistry on small ruthenium nanoparticles: evidence for site selective reactions and influence of ligands, Chem. Eur. J. 20 (2014) 1287–1297.

[32] P. Zhao, K. Ueda, R. Sakai, M. Ehara, A. Satsuma, S. Sakaki, Surface modification of MCr_2O_4 (M= Mg and Zn) by Cu-Doping: theoretical prediction and experimental observation of enhanced catalysis for CO oxidation, Appl. Surf. Sci. 605 (2022), 154681.

[33] S. Li, A.V. Nagarajan, D.R. Alfonso, M. Sun, D.R. Kauffman, G. Mpourmpakis, R. Jin, Boosting CO_2 electrochemical reduction with atomically precise surface modification on gold nanoclusters, Angew. Chem. Int. Ed. 60 (2021) 6351–6356.

[34] C.F. Xu, G.X. Chen, Y. Zhao, P.X. Liu, X.P. Duan, L. Gu, G. Fu, Y.Z. Yuan, N. F. Zheng, Interfacing with silica boosts the catalysis of copper, Nat. Commun. 9 (2018) 3367.

[35] J. Graciani, K. Mudiyanselage, F. Xu, A.E. Baber, J. Evans, S.D. Senanayake, D. J. Stacchiola, P. Liu, J. Hrbek, J.F. Sanz, J.A. Rodriguez, Highly active copper-ceria and copper-ceria-titania catalysts for methanol synthesis from CO_2, Science 345 (2014) 546–550.

[36] L.M. Martinez-Prieto, S. Carenco, C.H. Wu, E. Bonnefille, S. Axnanda, Z. Liu, P. F. Fazzini, K. Philippot, M. Salmeron, B. Chaudret, Organometallic ruthenium nanoparticles as model catalysts for CO hydrogenation: a nuclear magnetic resonance and ambient-pressure X-ray photoelectron spectroscopy study, ACS Catal. 4 (2014) 3160–3168.

[37] T.V. Heerden, E. van Steen, Metal–support interaction on cobalt based FT catalysts–a DFT study of model inverse catalysts, Faraday Discuss 197 (2017) 87–99.

[38] M. Akbari, A.A. Mirzaei, H. Atashi, Evaluation of reverse microemulsion parameters over the catalytic performance of promoted Fe–Co catalysts for the production of light olefins from syngas using box–behnken design, Catal. Lett. 149 (2019) 1305–1318.

[39] R. Zhang, L. Kang, H. Liu, B. Wang, D. Li, M. Fan, Crystal facet dependence of carbon chain growth mechanism over the Hcp and Fcc Co catalysts in the Fischer-Tropsch synthesis, Appl. Catal. B-Environ. 269 (2020), 118847.

[40] C.R.F. Lund, J.A. Dumesic, Strong oxide-oxide interactions in silica-supported magnetite catalysts. 1. X-ray diffraction and Mössbauer spectroscopy evidence for interaction, J. Phys. Chem. 85 (1981) 3175–3180.

[41] C.R.F. Lund, J.A. Dumesic, Strong oxide-oxide interactions in silica-supported magnetite catalysts. 2. The core/shell nature of the interaction, J. Phys. Chem. 86 (1982) 130–135.

[42] R.P. Mogorosi, N. Fischer, M. Claeys, E. van Steen, Strong-metal–support interaction by molecular design: fe–silicate interactions in Fischer–Tropsch catalysts, J. Catal. 289 (2012) 140–150.

[43] H. Hayashi, Z.C. Li, T. Tago, M. Kishida, K. Wakabayashi, Catalytic properties of Fe/SiO_2 catalysts prepared using microemulsion for CO hydrogenation, Appl. Catal. A-Gen. 231 (2002) 81–89.

[44] X. Liu, C. Zhang, Y.W. Li, J.W. Niemantsverdriet, J.B. Wagner, T.W. Hansen, Environmental transmission electron microscopy (ETEM) studies of single iron nanoparticle carburization in synthesis gas, ACS Catal. 7 (2017) 4867–4875.

[45] C. Yang, H.B. Zhao, Y.L. Hou, D. Ma, Fe_5C_2 nanoparticles: a facile bromide-induced synthesis and as an active phase for Fischer–Tropsch synthesis, J. Am. Chem. Soc. 134 (2012) 15814–15821.

[46] T.H. Pham, Y.Y. Qi, Y. Jia, X.Z. Duan, G. Qian, X.G. Zhou, D. Chen, W.K. Yuan, Insights into Hägg iron-carbide-catalyzed Fischer–Tropsch synthesis: suppression of CH_4 formation and enhancement of C–C coupling on χ-Fe_5C_2 (510), ACS Catal. 5 (2015) 2203–2208.

[47] J.X. Liu, H.Y. Su, D.P. Sun, B.Y. Zhang, W.X. Li, Crystallographic dependence of CO activation on cobalt catalysts: HCP versus FCC, J. Am. Chem. Soc. 135 (2013) 16284–16287.

[48] G. Kresse, J. Furthmüller, Efficiency of ab-initio total energy calculations for metals and semiconductors using a plane-wave basis set, Comput. Mater. Sci. 6 (1996) 15–50.

[49] G. Kresse, J. Furthmüller, Efficient iterative schemes for ab initio total-energy calculations using a plane-wave basis set, Phys. Rev. B 54 (1996) 11169–11186.

[50] P.E. Blochl, Projector augmented-wave method, Phys. Rev. B 50 (1994) 17953–17979.

[51] G. Kresse, From ultrasoft pseudopotentials to the projector augmented-wave method, Phys. Rev. B 59 (1999) 1758–1775.

[52] J.P. Perdew, K. Burke, M. Ernzerhof, Generalized gradient approximation made simple, Phys. Rev. Lett. 77 (1996) 3865–3868.

[53] M. Methfessel, A.T. Paxton, High-precision sampling for Brillouin-zone integration in metals, Phys. Rev. B 40 (1989) 3616–3621.

[54] J. Yin, X. Liu, X.W. Liu, H. Wang, H. Wan, S. Wang, W. Zhang, X. Zhou, B.T. Teng, Y. Yang, Y.W. Li, Z. Cao, X.D. Wen, Theoretical exploration of intrinsic facet-dependent CH_4 and C_2 formation on Fe_5C_2 particle, Appl. Catal. B 278 (2020), 119308.

[55] G. Henkelman, H. Jónsson, Improved tangent estimate in the nudged elastic band method for finding minimum energy paths and saddle points, J. Chem. Phys. 113 (2000) 9978–9985.

[56] J. Yin, M. Ehara, S. Sakaki, Single atom alloys vs. phase separated alloys in Cu, Ag, and Au atoms with Ni (111) and Ni, Pd, and Pt atoms with Cu (111): a theoretical exploration, Phys. Chem. Chem. Phys. 24 (2022) 10420.

[57] G. Henkelman, A. Arnaldsson, H.A. Jonsson, A fast and robust algorithm for Bader decomposition of charge density, Comput. Mater. Sci. 36 (2006) 354–360.

[58] (a) S. Nosé, A unified formulation of the constant temperature molecular dynamics methods, J. Chem. Phys. 81 (1984) 511–519;
(b) W.G. Hoover, Constant-pressure equations of motion, Phys. Rev. A 34 (1986) 2499–2500.

[59] S. Zhao, X.W. Liu, C.F. Huo, Y.W. Li, J.G. Wang, H.J. Jiao, Surface morphology of Hägg iron carbide (χ-Fe_5C_2) from ab initio atomistic thermodynamics, J. Catal. 294 (2012) 47–53.

[60] J.J. Retief, Powder diffraction data and rietveld refinement of Hägg-carbide, χ-Fe_5C_2, Powder Diffr. 14 (1999) 130–132.
[61] J.K. West, L.L. Hench, Molecular orbital models of silica rings and their vibrational spectra, J. Am. Ceram. Soc. 78 (1995) 1093–1096.
[62] L.T. Zhuravlev, The surface chemistry of amorphous silica. Zhuravlev model, Colloids Surf. A Physicochem. Eng. Asp. 173 (2000) 1–38.
[63] J. Yu, D. Mao, Q. Guo, G. Lu, Catalytic conversion of syngas into C_{2+} oxygenates over Rh/SiO_2-based catalysts: the remarkable effect of hydroxyls on the SiO_2, J. Mol. Catal. A-Chem. 367 (2013) 38–45.
[64] R.L. Mozzi, B.E. Warren, The structure of vitreous silica, J. Appl. Crystallogr. 2 (1969) 164–172.
[65] X.F. Yang, P. Roonasi, A.A. Holmgren, A study of sodium silicate in aqueous solution and sorbed by synthetic magnetite using in situ ATR-FTIR spectroscopy, J. Colloid Interface Sci. 328 (2008) 41–47.
[66] E. Vinogradova, M. Estrada, A. Moreno, Colloidal aggregation phenomena: spatial structuring of TEOS-derived silica aerogels, J. Colloid Interface Sci. 298 (2006) 209–212.
[67] Y. He, P. Zhao, Y. Meng, W. Guo, Y. Yang, Y.W. Li, C.F. Huo, X.D. Wen, Hunting the correlation between Fe_5C_2 surfaces and their activities on CO: the descriptor of bond valence, J. Phys. Chem. C 122 (2018) 2806–2814.
[68] T.H. Pham, X.Z. Duan, G. Qian, X.G. Zhou, D. Chen, CO activation pathways of Fischer–Tropsch synthesis on χ-Fe_5C_2(510): direct versus hydrogen-assisted CO dissociation, J. Phys. Chem. C 118 (2014) 10170–10176.
[69] C. Zheng, Y. Apeloig, R. Hoffmann, Bonding and coupling of C1 fragments on metal surfaces, J. Am. Chem. Soc. 110 (1988) 749–774.
[70] J. Cheng, P. Hu, P. Ellis, S. French, G. Kelly, C.M. Lok, An energy descriptor to quantify methane selectivity in Fischer− Tropsch synthesis: a density functional theory study, J. Phys. Chem. C 113 (2009) 8858–8863.
[71] J. Cheng, X.Q. Gong, P. Hu, C.M. Lok, P. Ellis, S. French, A quantitative determination of reaction mechanisms from density functional theory calculations: fischer–Tropsch synthesis on flat and stepped cobalt surfaces, J. Catal. 254 (2008) 285–295.
[72] E.S. Lox, G.F. Froment, Kinetics of the Fischer-Tropsch reaction on a precipitated promoted iron catalyst. 1. experimental procedure and results, Ind. Eng. Chem. Res. 32 (1993) 61–70.
[73] E.S. Lox, G.F. Froment, Kinetics of the Fischer-Tropsch reaction on a precipitated promoted iron catalyst. 2. Kinetic modeling, Ind. Eng. Chem. Res. 32 (1993) 71–82.
[74] J. Cheng, P. Hu, P. Ellis, S. French, G. Kelly, C.M. Lok, Chain growth mechanism in Fischer-Tropsch synthesis: a DFT study of C−C coupling over Ru, Fe, Rh, and Re surfaces, J. Phys. Chem. C 112 (2008) 6082–6086.
[75] J. Cheng, P. Hu, P. Ellis, S. French, G. Kelly, A DFT study of the chain growth probability in Fischer–Tropsch synthesis, J. Catal. 207 (2008) 221–228.
[76] J. Cheng, P. Hu, P. Ellis, S. French, G. Kelly, C.M. Lok, Density functional theory study of iron and cobalt carbides for Fischer−Tropsch synthesis, J. Phys. Chem. C 114 (2010) 1085–1093.
[77] J. Yin, Y. He, X. Liu, X. Zhou, C.F. Huo, W. Guo, Q. Peng, Y. Yang, H. Jiao, Y.W. Li, X.D. Wen, Visiting CH_4 formation and $C_1 + C_1$ couplings to tune CH_4 selectivity on Fe surfaces, J. Catal. 372 (2019) 217–225.
[78] R. Zhang, G. Wen, H. Adidharma, A.G. Russell, B. Wang, M. Radosz, M. Fan, C_2 oxygenate synthesis via Fischer–Tropsch synthesis on Co_2C and Co/Co_2C interface catalysts: how to control the catalyst crystal facet for optimal selectivity, ACS Catal. 7 (2017) 8285–8295.